ACS Chemical Neuroscience
Cite This: ACS Chem. Neurosci. 2019, 10, 3758−3768
Research Article
pubs.acs.org/chemneuro

Clinical Chemistry Route for Investigation of Alzheimer's Disease: A Label-Free Electrochemiluminescent Biosensor for Glycogen Synthase Kinase-3 Beta

Rong Tan,[†,∥] Hongying Cheng,[‡,∥] Huiling Li,[*,§] and Yifeng Tu[*,†]

[†]College of Chemistry, Chemical Engineering and Materials, Soochow University, Suzhou, 215123, P. R. China
[‡]School of Chemistry, Biology and Materials Engineering, Suzhou University of Science and Technology, Suzhou 215009, P. R. China
[§]College of Nursing, Soochow University, Suzhou, 215006, P. R. China

ABSTRACT: Herein, we report a novel label-free electrochemiluminescent (ECL) biosensor for the detection of glycogen synthase kinase-3 beta (GSK-3β). A simple and feasible sensor was prepared by a two-step process. A polymeric coordination layer of phosphorylated poly vinyl with Zr^{4+} was used as the sensory hosting matrix because it efficiently formed a complex. The exterior Zr^{4+} can further combine with another phosphate through coordination, and GSK-3β catalyzes the phosphorylation of protein molecules. Thus, the biosensor can detect GSK-3β using luminol as an ECL probe. The ECL intensity of the proposed sensor responded proportionally to the concentration of GSK-3β under direct immersion mode with a linear response in a logarithmic scale over the wide range from 0.5 to 91.5 ng L^{-1} and a detection limit of 0.055 ng L^{-1}. Excellent selectivity, stability, and reproducibility were achieved using the prepared biosensor, which has a simple preparation, low cost, and disposable suitability. This work aims to provide a novel tool for early diagnosis and pathological mechanism exploration about AD by detecting inchoate change of GSK-3β content in body fluid, thus to precaution the risk of Alzheimer's disease. It is of great importance for clinical chemistry for the investigation of Alzheimer's disease.

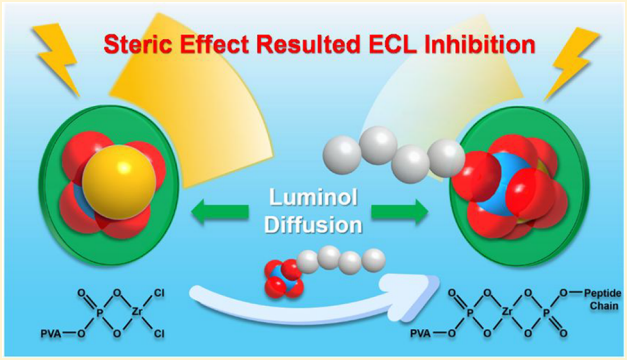

KEYWORDS: *Glycogen synthase kinase-3 beta, electrochemiluminescence, luminol, coordination, zirconium*

1. INTRODUCTION

Alzheimer's disease (AD) is a chronic neurodegenerative disease with common symptoms including cognitive capacity and behavioral issues, severely jeopardizing the physical and mental health of senior citizens. In addition, AD results in the loss of body functions eventually death due to the lack of effective medications and treatment methods currently available. Fortunately, clinicians can delay mental deterioration when AD is diagnosed and intervention begun at the early stages of the disease.[1−4] To date, AD has been shown to be associated with extracellular-amyloid (Aβ) plaques that damage the synapses and create neurofibrillary tangles (NFT).[5,6] Glycogen synthase kinase-3 (GSK-3) has been identified as a pivotal marker of neurodegeneration in AD. GSK-3 controls a wide range of biological processes, including the phosphorylation of the key τ-protein, an integral component of NFT deposits that disrupts neuronal function, and increases the production and deposition of Aβ.[7,8] However, the reliability of this description has been questioned recently due to the lack of solid data regarding the physiopathological aspects of GSK-3 in terms of distinguishing between healthy and diseased patients (AD) or dementia.[9] Therefore, determination of the function of GSK-3 in AD is absolutely necessary. GSK-3 contains two main subtypes, GSK-3α and GSK-3β, which exhibit 98% homology in their catalytic region.[10] However, these constructs are not functionally interchangeable because of the substantial differences in their N- and C-terminal sequences. As demonstrated by the embryonic-lethal phenotype when the gene encoding GSK-3β was knocked out, cell proliferation and metabolism is controlled by GSK-3β through a variety of signaling pathways including Wnt, Nuclear Factor kappa-B, Epidermal Growth Factor and insulin.[11] Furthermore, extensive experimental and clinical data have confirmed that GSK-3β is the predominant subtype, both physiologically and pathologically, and is expressed in most cells. Its expression levels can be monitored by the simple blood test, unlike GSK-3α which mainly expressed in sperm.[12] Thus, GSK-3β is now receiving widespread attention as a therapeutic target for the prevention and treatment of AD. More research is needed to more deeply

Received: May 11, 2019
Accepted: July 19, 2019
Published: July 19, 2019

DOI: 10.1021/acschemneuro.9b00278
ACS Chem. Neurosci. 2019, 10, 3758−3768

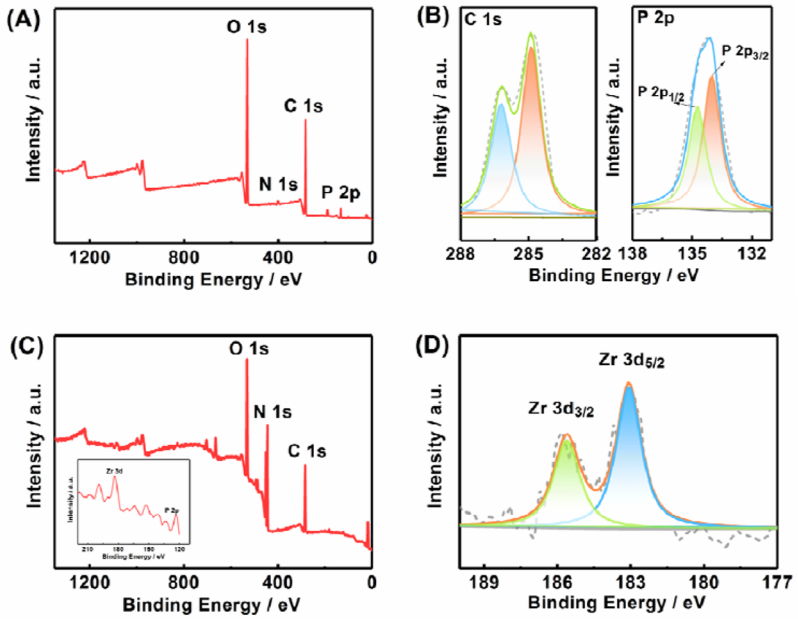

Figure 1. (A) The full scale XPS spectrum of PPVA; (B) the XPS analysis of the C_{1s} and P_{2p} orbits of PPVA; (C) the full scale XPS spectrum of the sensor matrix, the inset is an enlarged part; (D) the XPS analysis of Zr_{3d} orbit in the surface of the resultant sensor.

investigate τ-protein phosphorylation by obtaining more sensitive and accurate data as it is essential to determine its role in AD prognosis.[13−17] The development of novel methods for the detection of GSK-3β will also aid in the further understanding of AD.

Western blotting is the classical method for GSK-3β detection, but this method is limited by the cumbersome process and low sensitivity, although distinct and accurate results have been achieved.[18,19] De Simone et al. proposed an alternative method involving selective electrospray ionization quadrupole time-of-flight MS for the precise characterization of GSK-3β.[20] This method overcame the drawback related to isotope labeling to attain high sensitivity and reproducibility, but this method requires expensive instrumentation. In addition, while other methods such as quantitative real-time polymerase chain reaction and enzyme immunometric assay are available, they have their own distinct disadvantages.[21−24] Electrochemiluminescence (ECL) has attracted significant interest in recent years as a promising approach that can detect subtle changes of target, and has been adopted for clinical detection and investigation.[25−29] The detection of GSK-3β using ECL has been reported here for the first time. ECL was found to be an excellent detection system to monitor GSK-3β and it overcome the shortcomings of other methods.

As a commonly used water-soluble polymer, poly(vinyl alcohol) (PVA) is widely used in the biomimetic field. It can be firmly fixed to electrodes due to its inherent high cohesiveness.[30,31] After phosphorylation of the PVA, it can act as a substrate to impregnate Zr^{4+} to serve as a sensing matrix. Herein, the sensing response depended on the strong coordination of Zr^{4+} with another phosphate from protein phosphorylated by the action of GSK-3β. The inhibited ECL of luminol was used as an indicator to quantify the amount of GSK-3β present in the samples. Without the use of other linkers, a simple and label-free sensor was fabrication. In addition, the sensor output was triggered by the transfer dynamics of luminol rather than the chemical reaction, which was fundamental for the highly sensitive, controllable, and reproducible sensing properties of the device. This technology is capable of mass production for disposable devices, while it exhibits good stability, high sensitivity, and excellent reproducibility, meeting the requirements for clinical use.

2. RESULTS AND DISCUSSION

Present absence of clinical therapy for AD is a great challenge in the anthropic history of medicine. Early diagnosis is a top priority to prevent its exacerbation and the worst outcome. In this work, a biosensor, signaling through the coordination between Zr^{4+} and two phosphates, is proposed to detect a pivotal marker of AD - GSK-3β. With the aim to explore the pathological mechanism about AD, it can also provide an effective method for the early diagnosis of Alzheimer's disease. This is exactly an attempt about how to tie chemistry with biology disciplines more closely. We can predict that the simple preparation, low cost, and rapid detection of this biosensor meets the requirement for clinical application.

2.1. Verification and Optimization of the Biosensor Preparation. The phosphorylation degree of PVA must be determined to verify the function of phosphorylated PVA (PPVA) for final sensor performance. X-ray photoelectron spectroscopy (XPS) was used to confirm the formation of PPVA. Figure 1A shows the overall XPS spectrum with O 1s, N 1s, P 2p, and C 1s peaks. A doublet of P $2p_{3/2}$ and $2p_{1/2}$ peaks at 134.0 and 134.6 eV, respectively, arose from the P^{5+} state as deconvoluted from the spectrum of the P 2p electron (Figure 1B), demonstrating the successful phosphorylation of PVA. The chemical states of carbon are represented by the two fitted peaks in the C 1s peak at approximately 285.0 and 286.2 eV.[32,33] The 0.072 elemental ratio of P to C was achieved by calibrating their respective peak areas.

The functionalized interface of Zr^{4+}-PPVA acted as hosting matrix for sensing signaling. Therefore, optimization of the associated parameter were considered to achieve high performance. First, the influence of the amount of PPVA sprayed onto the electrode was investigated, showing negligible effect on ECL behavior. From the SEM-EDS mapping analysis

DOI: 10.1021/acschemneuro.9b00278
ACS Chem. Neurosci. 2019, 10, 3758−3768

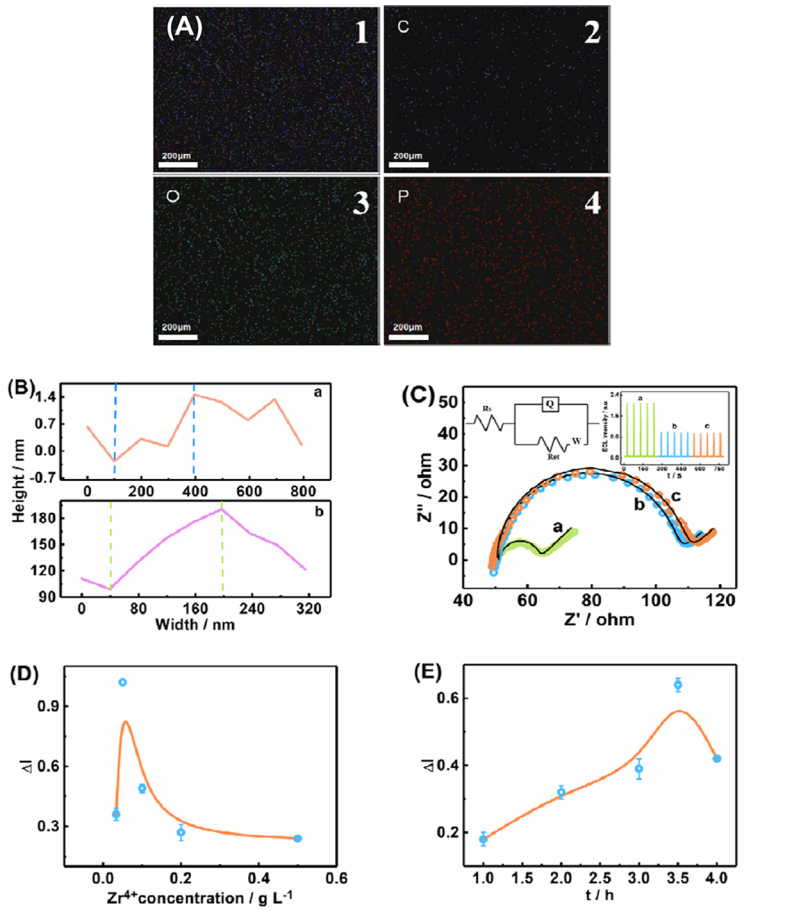

Figure 2. (A) The SEM-EDS mapping analysis of PPVA/ITO, pictures from 1 to 4 is of the all element, C, O, and P, respectively. (B) The different XZ data of loaded PPVA on ITO by ultrasonic atomization for (a) 1 min and (b) 15 min; (C) The EIS in 0.1 M KCl containing 5 mM $Fe(CN)_6^{3-}$, the inset is the corresponding ECL intensity, here the curve (a) is of bare ITO, (b) and (c) are the same as the two electrodes in (B); The optimization of the preparation conditions for Zr^{4+}/PPVA/ITO sensor including (D) the concentration of Zr^{4+} and (E) the duration of Zr^{4+} deposition.

which showed the surface distribution on the electrode surface (Figure 2A), the homogeneously distributed C, O, and P indicated a uniform layer of PPVA was obtained. With variation of the ultrasonic spraying time (from 1 to 15 min, Figure 2B), the thickness of this film can be adjusted from approximately 1.2 to 100 nm. The electrochemical impedance spectroscopy (EIS) curves in Figure 2C showed no significant change in electrochemical resistance (R_{et} of the electrodes were 54.7 ± 0.2 and 57.9 ± 0.4 for thickness difference of higher than 2 orders of magnitude), and did not induce notable differences in ECL emission (inset of Figure 2C). These results indicate the better conductivity of PPVA (measured to be 491 mS, owing to the electron-rich phosphate groups) is beneficial for improved and robust sensing ability. Thus, this parameter did not require further adjustment.

The concentration of the Zr^{4+} solution and its binding time on PPVA are important for the final performance of the sensor. By adjusted the parameters as shown in Figure 2D and 2E, 30 μL of 0.05 g L^{-1} Zr^{4+} loading onto the electrode at room temperature for 3.5 h produced optimal ECL behavior.

Under these optimized conditions for sensor fabrication, the microstructure of the electrode at every step was observed by microscopy. Compared with the SEM image of the bare ITO (image 1 in Figure 3A), the PPVA/ITO (image 2 in Figure 3A) showed a uniformly distributed layer on the electrode surface, indicating that ultrasonic atomization prevented the formation of a dense PPVA film, agreeing with the results shown in Figure 2A. From image 3 in Figure 3A, the morphology of Zr^{4+}/PPVA/ITO was more evenly dispersed because the coordination between Zr^{4+} and PO_4^{3-} changed the geometric microstructure of the macromolecular polymer.

The AFM topographic morphology further validated the above observations. Compared to the surface of bare ITO glass (image 1 in Figure 3B), a cellular granular structure was formed with deposited ITO particles. Afterward, spray coating of PPVA reduced the surface roughness (image 2 in Figure 3B) due to its flow ability and viscosity. After combination with Zr^{4+}, the surface dispersion became more uniform (image 3 in Figure 3B), as a result of the more balanced surface tension. These results preliminarily confirmed the success of sensor preparation.

Figures 1C shows the full-scale XPS spectrum of the resultant sensor, where peaks arising from O 1s, N 1s, P 2p, and Zr 3d were observed. The spectrum of Zr 3d (Figure 1D) is a doublet of the Zr $3d_{5/2}$ and $3d_{3/2}$ peaks of Zr^{4+}, at 183.0 and 185.4 eV, respectively, indicating the successful conglutination of Zr^{4+} on PPVA.[34] UV−vis spectrophotometry of the Zr^{4+} xylenol orange (XO) complex was used to determine the coverage of Zr^{4+} on the electrode surface. The absorption peak was measured at around 530 nm[35] (Figure 3C), and using

DOI: 10.1021/acschemneuro.9b00278
ACS Chem. Neurosci. 2019, 10, 3758−3768

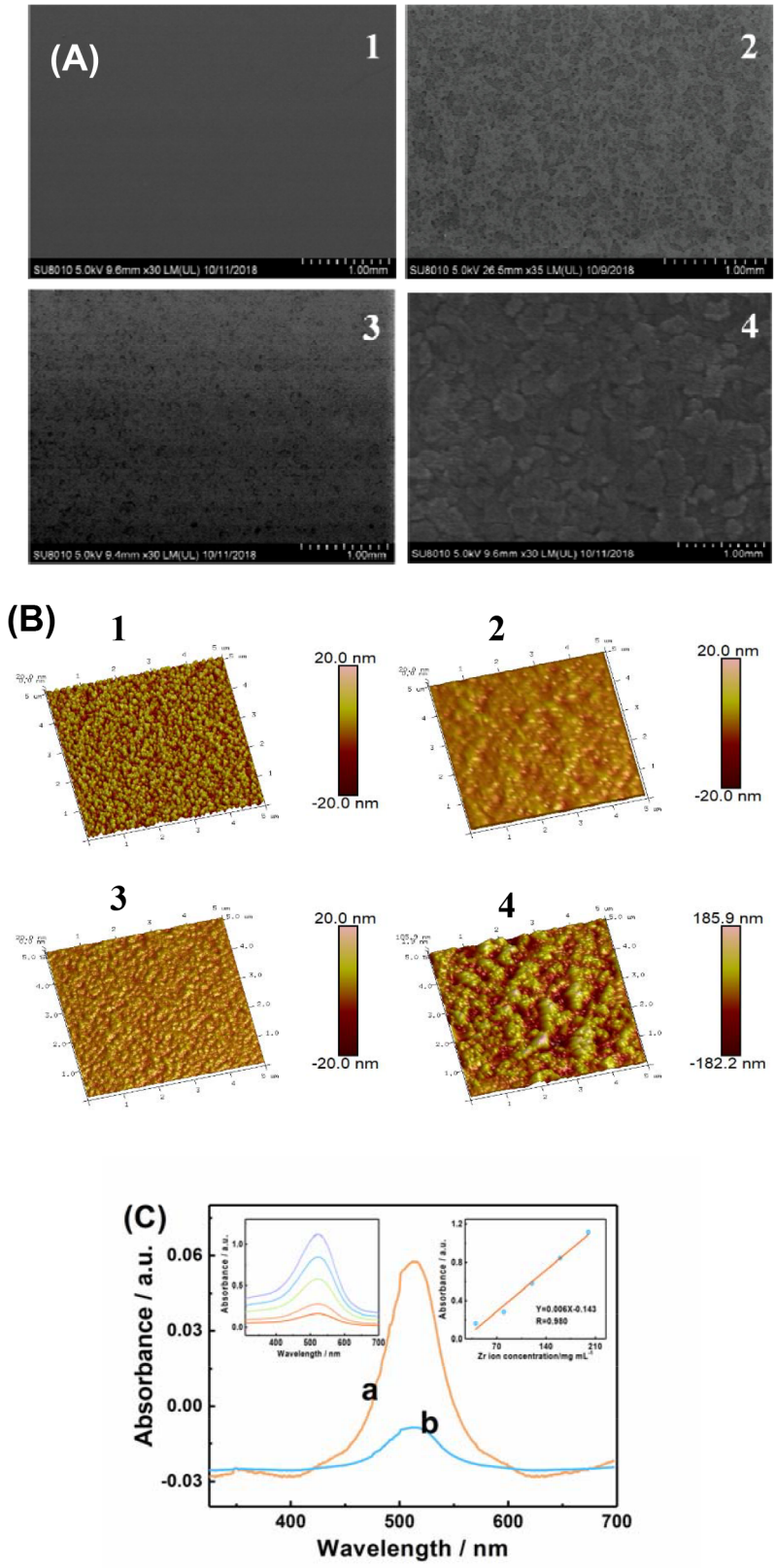

Figure 3. A) The SEM and (B) the AFM images (1) are ITO; (2) PPVA/ITO; (3) resultant sensor and (4) one after response occurred; (C) The UV−visible absorption spectrum of (a) resultant sensor and (b) the sensor after use, the inserted are the UV−vis spectra of standard solution of Zr^{4+} complex and the calibration curve.

standard calibration (inset of Figure 3C), the actual coverage of Zr^{4+} on the host matrix was roughly estimated to be at the level of microgram per cm^2, as layers of atoms.

2.2. Optimized Conditions for Sensing Performance.

The pH of the buffer solution significantly affected the sensing performance of the sensor. To balance the requirement for

DOI: 10.1021/acschemneuro.9b00278
ACS Chem. Neurosci. 2019, 10, 3758−3768

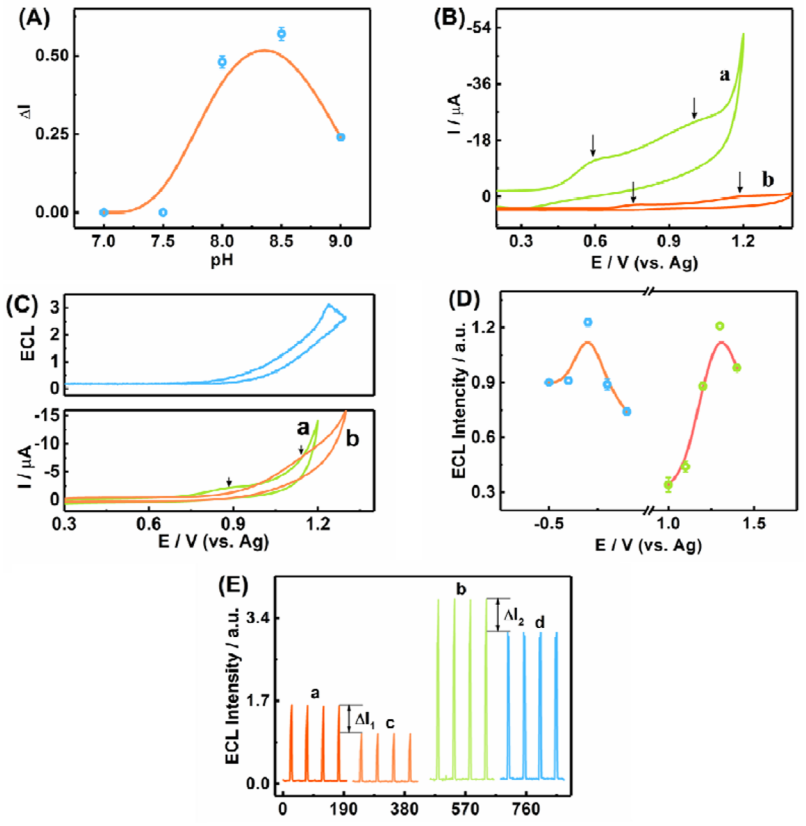

Figure 4. (A) The optimized conditions of buffered pH for ECL detection, $C_{Luminol} = 1.0 \times 10^{-7}$ M. The CVs of 2×10^{-4} M luminol on (B) Pt electrode and (C) ITO electrode in 0.2 M phosphate solution at (a) pH12 and (b) pH8.5, the first half of (C) is the corresponding ECL curve during one CV cycle; (D) The optimized conditions of supplied voltages, $C_{Luminol} = 1.0 \times 10^{-7}$ M. (E) The influence of oxygen on sensing output, maps a and b for sensor background at equilibrated oxygen or saturated oxygen respectively, c and d for same conditions but after responding to target.

high pH for strong ECL emission and neutral medium for protein survival, pH 8.5 was chosen after experimental optimization (Figure 4A).

The excitation potential is the central factor of the ECL response. According to the literature,[36−39] luminol can be oxidized by a two-step reaction in alkaline medium. The cyclic voltammetry (CV) showed that this reaction occurred at ca. 0.6 and 1.1 V using Pt as a working electrode at pH 12 (curve a in Figure 4B), in accordance with the previous reports. However, these potentials positively deviated to ca. 0.75 and 1.2 V at pH 8.5 (curve b in Figure 4B). In addition, the potentials were dependent on electrode material. Figure 4C shows that the first step oxidation of luminol on ITO glass occurred at approximately 0.9 V (curve a) or 1.2 V (curve b) under these two pH conditions, without a recordable second-step oxidation in the potential window. Meanwhile, a clear ECL emission trend during the CV process was recorded and found totally accompanied by the CV (the first half of Figure 4C), here the highest ECL emission appears around 1.2 V. The real applied electrolytic power is a pulsed potential, thus the upper and lower limiting potentials should be optimized. The optimization experiments showed that the ECL intensity reached a maximum at −0.3/1.2 V lower/upper limiting potentials (Figure 4D). Here, the upper limiting potential exactly coincided with the CV results.

Reactive oxygen species (ROSs) acted as a coreactant participating in the ECL process of luminol, thus the content of oxygen influenced the output of resultant sensor. As shown in Figure 4E, the ECL output of untapped sensor rose substantially after the oxygen inpouring for a certain time (from a to b), but it will also get an ascent after the responding to target (from c to d). The conclusive thing is there the responding value (ΔI_1 and ΔI_2) is basically unchanged. These experimental results indicate that the ECL of luminol was adjustable by different level of dissolved oxygen to accommodate the background, but the sensing response almost does not relate to oxygen. Our previous research have already discussed the mechanism of sensitized ECL of luminol by ROSs.[36−38] While the ROSs, including singlet oxygen ($^1O_2$), superoxide hydrogen (H_2O_2), superoxide radical ($O_2^{\cdot-}$), hydroxyl radical (·OH), inorganic or organic peroxides, etc., are increasing along with the incessant augment of oxygen, they can promote the oxidation of those luminol radical anions to emit higher light. This verdict has a two-side effects, to provide a higher level of background but may not stable enough because of the leakage of oxygen. In this work, we have chosen the state of oxygen equilibrium to get ascendant stability (2.7% of RSD, for 15 consecutive cyclic potential scans) with simple operation (have no use for oxygenation) because our sensor has competent sensitivity. As shown in these previous studies, the application of negative potential (−0.3 V lower limiting potential) can yield ROSs from dissolved oxygen and enhance the ECL of luminol.

2.3. Discussion of the Biosensor Sensing Mechanism.

The sensor output was mainly controlled by the transfer dynamics of luminol. Here the ECL emission on the sensor

DOI: 10.1021/acschemneuro.9b00278
ACS Chem. Neurosci. 2019, 10, 3758−3768

Scheme 1. Fabricating Procedure and Sensing Mechanism of Developed Sensor

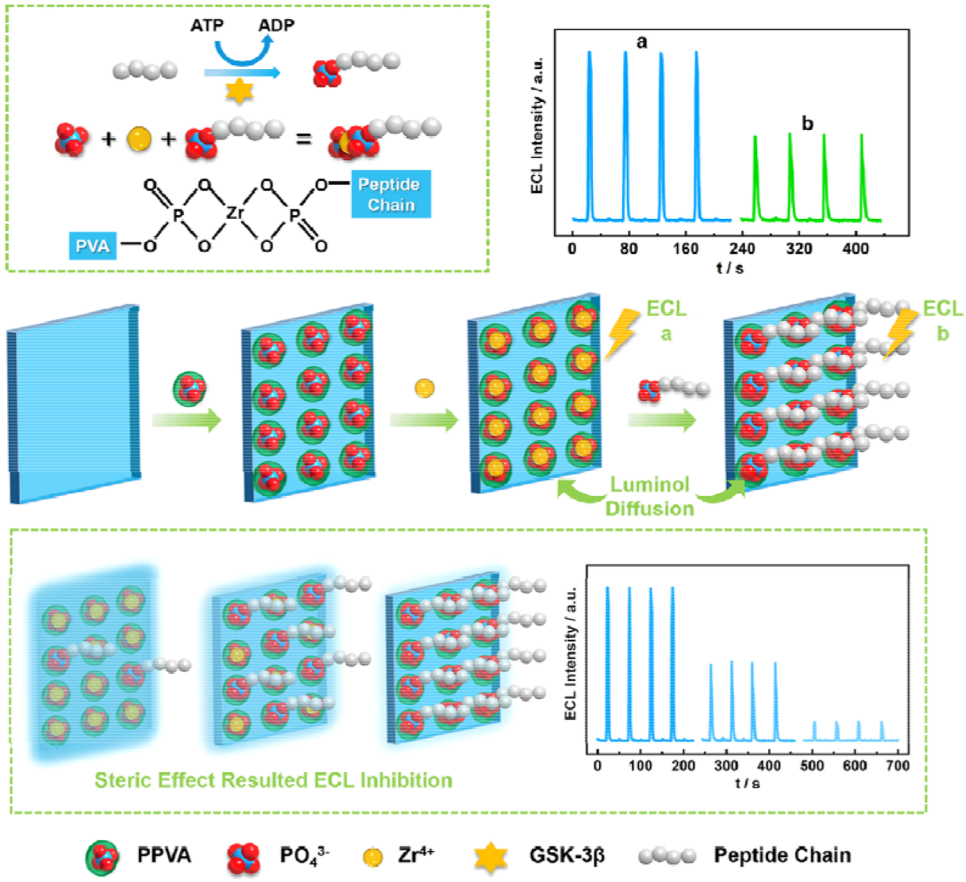

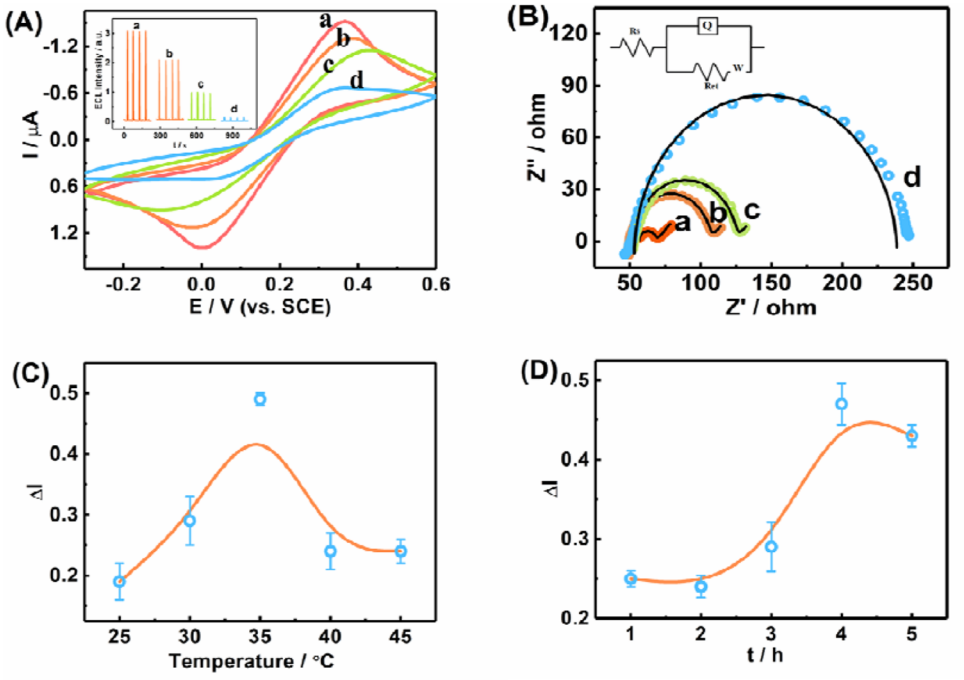

Figure 5. (A) CVs (50 mV s^{-1} of scan rate) and (B) EIS in 0.1 M KCl solution containing 5 mM of $Fe(CN)_6^{3-}$ for (a) bare ITO, (b) PPVA/ITO, (c) resultant sensor, and (d) one after response occurred, the inset in (A) is the corresponding ECL maps. The effect of (C) temperature and (D) duration for sensing response.

reflects the oxidation of luminol, which was controlled by the diffusion of luminol toward sensor surface. This diffusion controlled process will be disturbed by those effective factors including steric hindrance which resulted in the depressed

DOI: 10.1021/acschemneuro.9b00278
ACS Chem. Neurosci. 2019, 10, 3758−3768

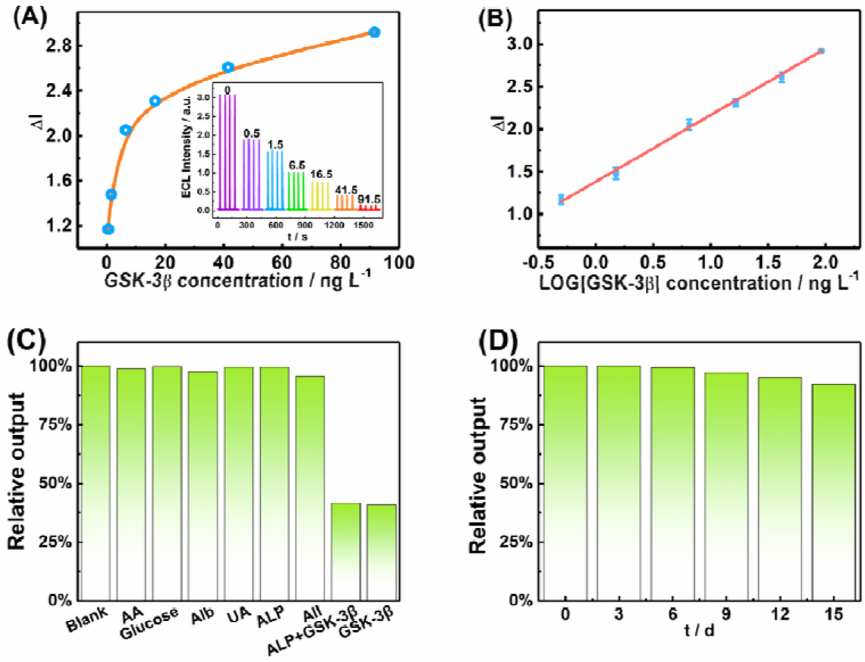

Figure 6. (A) The ECL response toward GSK-3β concentration, the inserted are the real ECL maps; (B) The calibration of the response vs. logarithm of GSK-3β concentration; (C) The ECL responses of the sensor upon potential interferences as AA, Glucose, Alb, UA, and ALP, $C_{Luminol}$ = 1.0 × 10^{-6} M, pH 8.5; (D) The stability of resultant sensor, 5 ng L^{-1} GSK-3β, $C_{Luminol}$ = 1.0 × 10^{-6} M, pH 8.5.

mass transfer rate of probe. As shown in Scheme 1, ITO was used as a substrate for the biosensor, given the cardinal number of ECL emission. When PPVA was dispersed on, the coating layer will obstruct the transfer of luminol toward the electrode, resulted in a small decrease in the ECL signal. Afterward, the Zr^{4+} directly incorporated through strong coordination ability, further impeded the diffusion of luminol toward the electrode surface, further decreasing the ECL emission. The balanced output (a) was considered to be the reference level for the sensor. When the phosphorylated proteins (p-proteins) yielded by the catalytic action of GSK-3β associated with the sensor, a higher degree of inhibition (b) was observed because of the giant spatial bulk of the proteins (as shown in the micrograph in image 4 of Figure 3A and image 4 of Figure 3B). The corresponding ECL maps are shown as an insert in Figure 5A. The gigantic spatial bulk of p-protein macromolecule has a great influence on the diffusion of luminol. As a direct measure of sensing output, the inhibition degree corresponded to the analyte concentration.

CV and EIS were used to verify the characteristics of the sensor to further understanding the underlying mechanism. The CV response of $Fe(CN)_6^{3-}$ on bare ITO (curve a in Figure 5A) showed a couple of well-defined reversible redox peaks. When PPVA was sprayed onto the substrate, the CV peak current was somewhat decreased (curve b in Figure 5A). After loading Zr^{4+}, the coupled electrons in the oxygen shell orbital in phosphate group will fill the vacant orbital of Zr^{4+}, coordinating the highly charged metal ion with PPVA and inducing lower electronic density on the electrode surface. This also results in poor electric conductivity, gradually reducing the redox peak current (curve c in Figure 5A). The peak current significantly decreased (curve d in Figure 5A) upon conjugation of the dielectric p-protein molecules formed by the catalytic action of GSK-3β.

Meanwhile the electron transfer resistance (R_{et}) was calculated by fitting the EIS data (Figure 5B) with the matched equivalent circuit. Values of 11.7 ± 0.5, 54.7 ± 0.2, 70.5 ± 0.2, and 185.2 ± 1.5 Ω were achieved for ITO, PPVA/ITO, Zr^{4+}/PPVA/ITO, and p-protein/Zr^{4+}/PPVA/ITO, respectively, corresponding to the CV and ECL tests.

2.4. Sensing Performance of the Resultant Sensor. Incubation conditions are important for sensing implementation: 35 °C (Figure 5C) and 4 h equilibration time (Figure 5D) for catalyzing protein phosphorylation and associated with the sensor were determined to be optimal. Under these conditions, the morphology of biosensor interface exhibited a noticeable change with many lumps appearing (Figure 3A(4)), and the surface roughness of the electrode significantly increased (Figure 3B(4)). This indicated that the macromolecular p-proteins were successfully combined with the sensor. It can also be demonstrated by UV−vis spectrophotometry of the Zr^{4+} - XO complexation. As is shown in Figure 3C, the absorption peak height around 530 nm decreased to "b" from "a", after the response. It demonstrates that the binding sites of Zr^{4+} were occupied by those phosphate groups of phosphorylated proteins.

Under the above-mentioned optimized experimental conditions, the ECL signal of the resultant sensor was monitored upon different concentrations of GSK-3β. The ECL intensity decreased with increasing GSK-3β concentration from 0.50 to 91.5 ng L^{-1} (insert curves in Figure 6A). This was attributed to the inhibition of ECL by the steric hindrance of those biomolecules which prevented diffusion of luminophores toward the sensor. Figure 6A shows the relationship between the response signal (ΔI) and GSK-3β concentration. The decreased ECL signal of the sensor showed a linear relationship with the logarithmic concentration of GSK-3β in this range (Figure 6B). The corresponding linear equation was determined to be Y= 1.38 + 0.783 log [GSK-3β] (r = 0.999). The detection limit was estimated to be 0.055 ng L^{-1} based on the response of three times the standard deviation of the zero-dose response. It is clear that the prepared sensor achieved

DOI: 10.1021/acschemneuro.9b00278
ACS Chem. Neurosci. 2019, 10, 3758−3768

improved performance, including lower detection limit and higher sensitivity than those developed in previous reports (Table 1),[20,24,40] which may be of great significance for the early detection of AD.

Table 1. Comparison of Detection Target and Detection Limit of Different Methods

method	detection target	detection limit	reference
ESI-QTOF	GSK-3β inhibitors	0.006 μM	20
EIA	GSK-3β concentration	74.4 ng L^{-1}	24
WB	Protein expression	unquantifiable detection	40
ECL biosensor	GSK-3β concentration	0.055 ng L^{-1}	this work

To evaluate the sensor selectivity, potential interferences were selected and investigated, including 1.5 μg L^{-1} ascorbic acid (AA), 1.5 μg L^{-1} glucose, 1.5 μg L^{-1} albumin (Alb), and 1.5 μg L^{-1} uric acid (UA). As is shown in Figure 6C, compared to 5 ng L^{-1} GSK-3β, the ECL signal variation from a single interferent or from the corresponding mixtures were all <10%, indicating that GSK-3β has a tolerance higher than 3000 times from those of high level interferents in blood or serum samples. In addition, an interference test using alkaline phosphatase (ALP), an enzyme that dephosphorylates the corresponding substrate, was performed. The experimental data showed no changes in the ECL signal when ALP was mixed with GSK-3β. It is reasonable to believe that the coordination of the p-protein with the sensor surface occurs as soon as it is generated, preventing dephosphorylation by phosphatase due to the shielded active site. Ultimately, as has been previously demonstrated,[41] dilution is the simplest method to prevent interference from unknown potential interferents. This technique can be used to prevent interference in the developed sensor because of its ultrahigh sensitivity. Regrettably, since GSK-3α and GSK-3β are highly homologous and can catalyze the phosphorylation of same protein, the biosensor developed herein cannot achieve high selectivity between them.[42] However, GSK-3α is mainly expressed in sperm, is not commonly expressed along with GSK-3β. Of course, if necessary, separation techniques such as electrophoresis can be used to eliminate GSK-3α from the sample of interest.

Five parallel sensors from the same batch were used to detect 5 ng L^{-1} GSK-3β to determine the reproducibility of the sensor. The relative standard deviation was 3.1%, indicating adequate performance. In addition, the stability of the prepared biosensor was tested using 5 ng L^{-1} GSK-3β every 3 days for 15 days using a single sensor, preserved in phosphate buffered saline (PBS) at 4 °C when not in use. As shown in Figure 6D, the sensor response showed no significant changes from the initial response, indicating that the proposed sensor was reliable.

2.5. the Actual Sample Detection by the Biosensor. the biosensor was tested to confirm its practicability by detecting the GSK-3β in human serum samples. The serum sample (diluted 500 times) of three volunteers were obtained, tested, and compared with the standard ELISA method. As shown in Table 2, the results were very similar, indicating the accuracy of the novel sensor. Here, as we all know, there are lots of phosphates present in blood or serum samples, and the exterior Zr^{4+} of the biosensor can also coordinate with them. Whether these occupied binding sites would impact the ECL emission of sensor is worth of consideration, but the experimental results showed no significant changes from the initial response. So it is inferable that the action of ionic phosphate is insignificant to induce steric hindrance, having no effect on the diffusion of luminol. In addition, it is easier to coordinate with metal ion for p-protein because of higher density of electron cloud on P═O bond due to the electron transfer via $\sigma-\pi$ conjugation. Thus, the p-proteins can be as expected to substitute those phosphate ions to realize the sensing outcome. Recovery tests were conducted by the standard addition method, with the results ranging from 84.0% to 104% (see Table 3), indicating that the prepared sensor exhibited reliable analytical performance.

Table 2. Detected Results in Samples

sample no.	ECL biosensor detected[a] ng L^{-1}	ELISA ng L^{-1}	RD %
1	1757.3	1647.0	3.24
2	2486.2	2382.0	2.14
3	2029.5	1912.0	2.98

[a]The detections were carried on after 500-folds dilution.

Table 3. Detected Recoveries of GSK-3β in a Diluted Serum Sample

GSK-3β in sample ng L^{-1}	GSK-3β added ng L^{-1}	found ng L^{-1}	recovery %	RSD %, n = 5
6.70	1.00	7.54	84.00	2.29
	3.00	9.26	85.33	2.38
	5.00	11.38	93.60	3.12
	10.00	17.18	104.80	3.68

3. CONCLUSION

GSK-3β is a very conserved serine/threonine kinase in evolution and is necessary for protein phosphorylation. Its typical substrates are signaling proteins, structural proteins, and transcription factors, which regulate cell differentiation and proliferation. Recently, studies have implicated GSK-3β in AD. Herein, we developed an ECL biosensor for GSK-3β detection with excellent analytical performance, providing a novel method for AD researchers to understand its pathological mechanism. Furthermore, because of its ultrahigh detection sensitivity, the prepared sensor may be able to detect the tiny changes in GSK-3β concentrations to predict the risk of AD, so that patients can receive an accurate diagnosis and intervention can begin as early as possible.

4. METHODS

4.1. Reagents and Materials. ITO thin film coated glass was purchased from Guluo Glass Co., Ltd. (Henan, China, http://www.guluoglass.com/). It is used as basal working electrode after cut into dimension of 1.0 cm × 5.0 cm for each piece; its working area is controlled for 1 cm^2 by insulating tape to cover excrescent portion. Luminol was obtained from Fluka (U.S., http://www.fluka.org/). Poly(vinyl alcohol) (PVA) was purchased from Sinopharm Chemical Reagent Co., Ltd. (China, https://www.sinoreagent.com/). Glycogen synthase kinase-3 beta (GSK-3β) was purchased from Lifes Biological Laboratory Equipment Co., Ltd. (Wuxi, China, http://www.lifesbiology.com/). Phosphoric acid (H_3PO_4), carbamide, ethanol, and other chemicals were of analytical grade and purchased from Chinasun Specialty Products Co., Ltd. (Changshu, China, http://www.qschem.com/). All solutions were prepared using ultrapure water (18.2 MΩ·cm). Following buffered solutions were used in this study: GSK-3β reaction buffer (H-buffer; 50 mM HEPES, 0.5 mM

DOI: 10.1021/acschemneuro.9b00278
ACS Chem. Neurosci. 2019, 10, 3758−3768

adenosine triphosphate(ATP), 1 g/L bovine serum albumin (BSA), pH 7.4); ECL buffer (E-buffer; 0.02 M PBS, 1×10^{-6} M luminol, pH 8.5).

Proteins that contain the Ser/Thr(P0)×××Ser/Thr(P+4) motif are the native substrates of GSK-3β.[43] The τ-protein is one of the major substrates after prephosphorylation. BSA (containing anamino acid sequence of LLFSSAYSRG with an S×××S section) was used as a substitute substrate herein. This was completely consistent with the identified sequence and was cheaper.[44]

4.2. Instruments. As described in detail in a previous paper, the ECL investigation was performed using a lab-built installation (the voltage of PMT used in the work is −1000 V).[45] Scanning electron microscopy (SEM) was performed using an S-4700 SEM instrument (Hitachi, Japan). Atomic force microscopy (AFM) (Dimension icon, Bruck, Germany) was used to observe the distribution and morphology of the electrode surface. X-ray photoelectron spectra (XPS) were collected using an ESCALAB 250Xi spectrometer (Thermo Scientific, U.S.). The cyclic voltammetry (CV) and electrochemical impedance spectroscopy (EIS) were measured using an RST-5200 Electrochemical Workstation (Suzhou Risetest Electronic Co., Ltd., China). ITO coated glass was used as a basal working electrode, Pt wire as a counter electrode, and saturated calomel electrode (SCE) as a reference electrode.

4.3. Preparation of the PPVA. PPVA was prepared according to a literature method.[46−48] Briefly, 2.0 g of PVA, 10 mL of phosphoric acid (85%, w/w), and 1.0 g of carbamide were mixed with 10 mL of ultrapure water and heated to 90 °C with constant magnetic stirring for 3 h to esterify the PVA with phosphoric acid. The solution was then cooled to room temperature and the solid matter was separated by pouring in 50 mL of ethanol slowly with stirring. The sample was then filtered and washed with ethanol several times to remove excess phosphoric acid and carbamide, affording the desired PPVA.

4.4. Fabrication of the Sensor. The ITO substrate was washed with acetone, ultrapure water, acetone, ultrapure water (30 min each) in sequence under ultrasonication, followed by drying under a nitrogen stream. Subsequently, 0.1 g of PPVA was added to 2 mL of water and heated to 90 °C under stirring until totally dissolved. The obtained hydrosol was scattered uniformly onto the ITO by ultrasonic atomization and 30 μL of Zr^{4+}solution was dropped onto the surface and equilibrated for 3.5 h to prepare the Zr^{4+}/PPVA/ITO sensor. The device was then rinsed with ultrapure water and dried with N_2.

4.5. ECL sensing. ECL investigation and determination of GSK-3β were performed using the lab-built quartz ECL cell containing the prepared sensor, Pt wire, Ag wire as the working, counter, and reference electrodes, respectively.[41,49] The ECL emission of luminol was generated when an impulse voltage was applied to the working electrode, then recorded after being converted to an electrical signal by the photomultiplier tube.[50] Afterward, 30 μL of H-buffer containing GSK-3β was spread onto the surface of sensor and allowed to equilibrate for 4 h at 35 °C to ensure complete reaction, then rinsed and dried. After this process, decreased ECL behavior of luminol on sensor in E-buffer was observed. The decreased ECL intensity (ΔI) was recorded as the sensing signal versus the background of ECL emission of luminol on a blank sensor. Under the optimized conditions, the response of the sensing signal was investigated as a function of GSK-3β concentration.

AUTHOR INFORMATION

Corresponding Authors

*(H.L.) E-mail: lhl8543@126.com.

*(Y.T.) E-mail: tuyf@suda.edu.cn.

ORCID

Yifeng Tu: 0000-0002-9630-4986

Author Contributions

R.T. designed and carried out experiments, analyzed experimental results, drafted and revised the manuscript; H.C. participated in experiments, analyzed experimental results, drafted the manuscript; H.L. associated director of this work, adviser on medical exploration, participated in the discussion and gave unique insights, directed the paper writing; Y.T. director of this work, designed the experiments, examined and analyzed the experimental results, directed the paper writing, revised and finalized the manuscript.

Author Contributions

‖R.T. and H.C. contributed equally.

Notes

The authors declare no competing financial interest.

ACKNOWLEDGMENTS

This work is financially supported by the National Natural Science Foundation of China (21675115, 21375091).

REFERENCES

(1) Zhu, H., Zhou, P., Alcauter, S., Chen, Y., Cao, H., Tian, M., Ming, D., Qi, H., Wang, X., Zhao, X., He, F., Ni, H., and Gao, W. (2016) Changes of intranetwork and internetwork functional connectivity in Alzheimer's disease and mild cognitive impairment. *J. Neural. Eng. 13* (4), 046008.

(2) Snowdon, D. A. (1997) Brain infarction and the clinical expression of Alzheimer disease: The nun study. *J. A. M. A 277* (10), 813−817.

(3) Morris, J. C., Storandt, M., Miller, J. P., McKeel, D. W., Price, J. L., Rubin, E. H., and Berg, L. (2001) Mild cognitive impairment represents early-stage Alzheimer disease. *Arch. Neurol. 58* (3), 397−405.

(4) Godyn, J., Jonczyk, J., Panek, D., and Malawska, B. (2016) Therapeutic strategies for Alzheimer's disease in clinical trials. *Pharmacol. Rep. 68* (1), 127−138.

(5) Nakamura, A., Kaneko, N., Villemagne, V. L., Kato, T., Doecke, J., Dore, V., Fowler, C., Li, Q. X., Martins, R., Rowe, C., Tomita, T., Matsuzaki, K., Ishii, K., Ishii, K., Arahata, Y., Iwamoto, S., Ito, K., Tanaka, K., Masters, C. L., and Yanagisawa, K. (2018) High performance plasma amyloid-beta biomarkers for Alzheimer's disease. *Nature 554* (7691), 249−254.

(6) Rice, H. C., Malmazet, D., Schreurs, A., Frere, S., Molle, I. V., Volkov, A. N., Creemers, E., Vertkin, I., Nys, J., and Ranaivoson, F. (2018) Secreted amyloid-β precursor protein functions as a GABABR1a ligand to modulate synaptic transmission. *Alzheimer's Dementia 363* (6423), 143−150.

(7) Li, L., Liu, Z., Liu, J., Tai, X., Hu, X., Liu, X., Wu, Z., Zhang, G., Shi, M., and Zhao, G. (2013) Ginsenoside Rd attenuates beta-amyloid-induced tau phosphorylation by altering the functional balance of glycogen synthase kinase 3beta and protein phosphatase 2A. *Neurobiol. Dis. 54*, 320−328.

(8) Takashima, A. (2006) GSK-3 is essential in the pathogenesis of Alzheimer's disease. *J. Alzheimer's Dis. 9*, 309−317.

(9) Kremer, A., Louis, J. V., Jaworski, T., and Van, L. F. (2011) GSK3 and Alzheimer's disease: facts and fiction. *Front. Mol. Neurosci. 4*, 17−27.

(10) Chen, X., Wang, R., Liu, X., Wu, Y. M., Zhou, T., Yang, Y. J., Perez, A., Chen, Y. C., Hu, L., Chadarevian, J. P., Assadieskandar, A., Zhang, C., and Ying, Q. L. (2017) A chemical-genetic approach reveals the distinct roles of GSK3 alpha and GSK3 beta in regulating embryonic stem cell fate. *Dev. Cell 43* (5), 563−566.

(11) Wang, J., Wu, Q., GRUNDKE-IQBAL, Alan, S., and Khalid, I. (1999) Study on phosphorylation of τ-protein by glycogen synthetase kinase-3. *J. Biochem. Mol. Biol. 15* (4), 589−592.

(12) Hugon, J., Mouton-Liger, F., Cognat, E., Dumurgier, J., and Paquet, C. (2018) Blood-Based Kinase Assessments in Alzheimer's Disease. *Front. Aging Neurosci. 10*, 338−344.

(13) Zou, Q. F., Hou, Y., Shen, F., and Wang, Y. Z. (2013) Polarized regulation of glycogen synthase kinase-3 beta is important for glioma cell invasion. *PLoS One 8* (12), 13−18.

(14) Ferrer, I., Gomez-Isla, T., Puig, B., Freixes, M., Ribé, E., Dalfo, E., and Avila, J. (2005) Current advances on different kinases involved

DOI: 10.1021/acschemneuro.9b00278
ACS Chem. Neurosci. 2019, 10, 3758−3768

in tau phosphorylation, and implications in Alzheimer's disease and tauopathies. *Curr. Alzheimer Res. 2*, 3−18.
(15) Hye, A., Kerr, F., Archer, N., Foy, C., Poppe, M., Brown, R., Hamilton, G., Powell, J., Anderton, B., and Lovestone, S. (2004) Glycogen synthase kinase-3 is increased in white cells early in Alzheimer's disease. *Neurosci. Lett. 373* (1), 1−4.
(16) Hurtado, D. E., Molina-Porcel, L., Carroll, J. C., MacDonald, C., Aboagye, A. K., Trojanowski, J. Q., and Lee, V. M. Y. (2012) Selectively silencing GSK-3 isoforms reduces plaques and tangles in mouse models of Alzheimer's disease. *J. Neurosci. 32* (21), 7392−7402.
(17) Nagao, M., and Hayashi, H. (2009) Glycogen synthase kinase-3beta is associated with Parkinson's disease. *Neurosci. Lett. 449* (2), 103−107.
(18) SoukhakLari, R., Moezi, L., Pirsalami, F., Ashjazadeh, N., and Moosavi, M. (2018) Curcumin ameliorates scopolamine-induced mice memory retrieval deficit and restores hippocampal p-Akt and p-GSK-3beta. *Eur. J. Pharmacol. 841*, 28−32.
(19) Sha, J., Zhang, H., Zhao, Y., Feng, X., Hu, X., Wang, C., Song, M., and Fan, H. (2019) Dexmedetomidine attenuates lipopolysaccharide-induced liver oxidative stress and cell apoptosis in rats by increasing GSK-3beta/MKP-1/Nrf2 pathway activity via the alpha2 adrenergic receptor. *Toxicol. Appl. Pharmacol. 364*, 144−152.
(20) Angela, D., Jessica, F., Marina, N., Annalisa, D., Vincenzo, T., Andrea, M., and Vincenza, A. (2017) Application of an ESI-QTOF method for the detailed characterizationof GSK-3 inhibitors. *J. Pharm. Biomed. Anal. 144*, 159−166.
(21) Gao, F. J., Hebbar, S., Gao, X. A., Alexander, M., Pandey, J. P., Walla, M. D., Cotham, W. E., King, S. J., and Smith, D. S. (2015) GSK-3beta phosphorylation of cytoplasmic dynein reduces Ndel1 binding to intermediate chains and alters dynein motility. *Traffic 16* (9), 941−961.
(22) Pandey, G. N., Rizavi, H. S., Tripathi, M., and Ren, X. (2015) Region-specific dysregulation of glycogen synthase kinase-3beta and beta-catenin in the postmortem brains of subjects with bipolar disorder and schizophrenia. *Bipolar Disord. 17* (2), 160−171.
(23) Wang, J., Lei, W., Li, G., Ma, H., Guo, H., and Li, S. (2019) CD151 promotes proliferation and migration of SK-NEP-1 cells via the GSK-3 beta/P21/cyclinD signaling pathway. *Pathol., Res. Pract. 215* (2), 329−334.
(24) Munkholm, K., Miskowiak, K. W., Jacoby, A. S., Vinberg, M., Leme Talib, L., Gattaz, W. F., and Kessing, L. V. (2018) Glycogen synthase kinase-3beta activity and cognitive functioning in patients with bipolar I disorder. *Eur. Neuropsychopharmacol. 28* (3), 361−368.
(25) Arun, A., Jan, C., Werner, E., and Andreas, M. (2001) A wireless electrochemiluminescence detector applied to direct and indirect detection for electrophoresis on a microfabricated glass device. *Anal. Chem. 73* (14), 3282−3288.
(26) Chovin, A., Garrigue, P., and Sojic, N. (2004) Electrochemiluminescent detection of hydrogen peroxide with an imaging sensor array. *Electrochim. Acta 49* (22−23), 3751−3757.
(27) Zheng, X., Guo, Z., and Zhang, Z. (2001) Flow-injection electrogenerated chemiluminescence determination of epinephrine using luminol. *Anal. Chim. Acta 441*, 81−86.
(28) Miao, P., Ning, L., Li, X., Li, P., and Li, G. (2012) Electrochemical strategy for sensing protein phosphorylation. *Bioconjugate Chem. 23* (1), 141−145.
(29) Richter, M. M. (2004) Electrochemiluminescence (ECL). *Chem. Rev. 104* (6), 3003−3036.
(30) Koski, A., Yim, K., and Shivkumar, S. (2004) Effect of molecular weight on fibrous PVA produced by electrospinning. *Mater. Lett. 58* (3−4), 493−497.
(31) Salavagione, H. J., Martinez, G., Gomez, R., and Segura, J. L. (2010) Synthesis of water-soluble perylenediimide-functionalized polymer through esterification with poly(vinyl alcohol). *J. Polym. Sci., Part A: Polym. Chem. 48* (16), 3613−3622.
(32) John, W., and Sons, C. (1993) High-resolution XPS of organic polymers: The scienta ESCA300 database. *Sur. Interface Anal. 20*, 267−267.
(33) Barrios, D., Vergaz, R., Sánchez-Pena, J. M., García-Cámara, B., Granqvist, C. G., and Niklasson, G. A. (2015) Simulation of the thickness dependence of the optical properties of suspended particle devices. *Sol. Energy Mater. Sol. Cells 143*, 613−622.
(34) Tan, M., Liu, Q., Zhang, N., Hu, H., Li, B., and Kang, X. (2011) Characterization of the surface film on Zr-based bulk metallic glass using X-ray photoelectron spectroscopy (XPS) and scanning electron microscopy (SEM). *J. Alloys Compd. 509* (19), 5926−5930.
(35) Yang, H., Wang, L., and Ma, X. (2005) Determination of zirconium amount in catalysts by xylenol orange spectrophotometry. *Liaoning Chem. Ind. 34* (7), 351−357.
(36) Ming, L., Peng, T., and Tu, Y. (2016) Multiple enhancement of luminol electrochemiluminescence using electrodes functionalized with titania nanotubes and platinum black: ultrasensitive determination of hydrogen peroxide, resveratrol, and dopamine. *Microchim. Acta 183* (1), 305−310.
(37) Yu, Z., Wei, X., Yan, J., and Tu, Y. (2012) Intensification of electrochemiluminescence of luminol on TiO_2 supported Au atomic cluster nano-hybrid modified electrode. *Analyst 137* (8), 1922−1929.
(38) Chu, H., Guo, W., Di, J., Wu, Y., and Tu, Y. (2009) Study on sensitization from reactive oxygen species for electrochemiluminescence of luminol in neutral medium. *Electroanalysis 21* (14), 1630−1635.
(39) Li, M., Gao, H., Wang, X., Wang, Y., Qi, H., and Zhang, C. (2017) A fluorine-doped tin oxide electrode modified with gold nanoparticles for electrochemiluminescent determination of hydrogen peroxide released by living cells. *Microchim. Acta 184* (2), 603−610.
(40) Sharma, A. K., Kumar, A., Sahu, M., Sharma, G., Datusalia, A. K., and Rajput, S. K. (2018) Exercise preconditioning and low dose copper nanoparticles exhibits cardioprotection through targeting GSK-3beta phosphorylation in ischemia/reperfusion induced myocardial infarction. *Microvasc. Res. 120*, 59−66.
(41) Ma, X., Fang, C., Yan, J., Zhao, Q., and Tu, Y. (2018) A label-free electrochemiluminescent immunosensor for glutamate decarboxylase antibody detection on AuNPs supporting interface. *Talanta 186*, 206−214.
(42) Jin, Y. H., Kim, H., Oh, M., Ki, H., and Kim, K. (2009) Regulation of Notch1/NICD and Hes1 expressions by GSK-3 alpha/beta. *Mol. Cells 27* (1), 15−19.
(43) Yoshimura, T., Kawano, Y., Arimura, N., Kawabata, S., Kikuchi, A., and Kaibuchi, K. (2005) GSK-3 beta regulates phosphorylation of CRMP-2 and neuronal polarity. *Cell 120* (1), 137−149.
(44) Tyan, Y. C., Yang, M. H., Liao, P. C., Liao, J. D., Jong, S. B., Liu, C. Y., Wang, M. C., and Grunze, M. (2007) MALDI-TOF MS sample preparation by using alkanethiolate self-assembled monolayers: A preliminary application for protein sample analysis. *Int. J. Mass Spectrom. 262* (1−2), 67−72.
(45) Zhai, S., Fang, C., Yan, J., Zhao, Q., and Tu, Y. (2017) A label-free genetic biosensor for diabetes based on AuNPs decorated ITO with electrochemiluminescent signaling. *Anal. Chim. Acta 982*, 62−71.
(46) Jeong, D., Cho, K., Lee, C., Lee, S., and Bae, H. (2016) Integration of forward osmosis process and a continuous airlift nitrifying bioreactor containing PVA/alginate- immobilized cells. *Chem. Eng. J. 306*, 1212−1222.
(47) Saat, A. M., and Johan, M. R. (2016) Enhanced thermal and structural properties of partially phosphorylated polyvinyl alcohol - Aluminum phosphate (PPVA-$AlPO_4$) nanocomposites with aluminium nitrate source. *AIP Conf. Proc. 1901*, 130011.
(48) Liu, N., W, L., Qiu, H., Yu, Y., Wang, H., and Zhu, B. (2013) Preparation of perlite-phosphorylated polyvinyl alcohol and its degradation characteristics of atrazine. *Sci. Technol. Rev. 31* (14), 15−21.
(49) Liu, X., Fang, C., Yan, J., Li, H., and Tu, Y. (2018) A sensitive electrochemiluminescent biosensor based on AuNP-functionalized ITO for a label-free immunoassay of C-peptide. *Bioelectrochemistry 123*, 211−218.
(50) Zhou, H., Gan, N., Hou, J., Li, T., and Cao, Y. (2012) Enhanced electrochemiluminescence employed for the selective

DOI: 10.1021/acschemneuro.9b00278
ACS Chem. Neurosci. 2019, 10, 3758−3768

detection of methyl parathion based on a zirconia nanoparticle film modified electrode. *Anal. Sci. 28* (3), 267−267.

DOI: 10.1021/acschemneuro.9b00278
ACS Chem. Neurosci. 2019, 10, 3758−3768